ACS OMEGA

Open Access

http://pubs.acs.org/journal/acsodf

Article

Experimental Investigation of Calcium-Doped Zinc Aluminate Nanoparticles as a Promising Material for Microwave Applications

Sekhar Didde, Raghvendra Sarvjeet Dubey,* Sampad Kumar Panda, and Gandla Satheesh Babu

Cite This: *ACS Omega* 2023, 8, 38064−38071

Read Online

ACCESS | Metrics & More | Article Recommendations

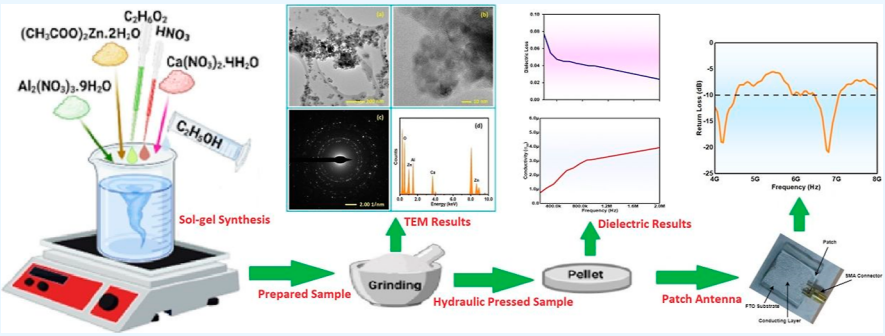

ABSTRACT: Miniaturization of microstrip patch antennas (MPAs) is vital in applications such as wireless networks, mobile devices, global positioning satellites, and upcoming wireless terminals. This miniaturization has led to a demand for new materials with higher permittivity compared to the existing ones. Zinc aluminate ($ZnAl_2O_4$) ceramic is an exceptional and versatile material in this context, thanks to its high dielectric permittivity and low tangent loss, making it suitable for microwave applications. This article explores the feasibility of sol−gel-prepared Ca-doped $ZnAl_2O_4$ ceramic nanoparticles to be useful in fabricating a MPA. These nanoparticles were examined using X-ray diffraction, which confirmed their polycrystalline structure, and the morphological investigation evidenced the spherical grains having a mean diameter of 16 nm. The dielectric permittivity of the $ZnAl_2O_4Ca$ nanoparticles is 21.11, with a tangential loss of 0.0247. A prototype MPA made by using Ca-doped $ZnAl_2O_4$ nanoparticles showed a return loss of −20.92 dB at a resonance frequency of 6.8 GHz with a bandwidth of 600 MHz. These results indicate that Ca-doped $ZnAl_2O_4$ ceramic nanoparticles possess exceptional dielectric characteristics, which make them a promising candidate for MPA applications.

1. INTRODUCTION

The field of microwave engineering is constantly evolving, and researchers are always looking for new materials with exceptional properties that can be used for various microwave applications. Zinc aluminate ($ZnAl_2O_4$) nanoparticles have gained significant attention due to their unusual characteristics and potential applications in various fields. These nanoparticles are thermally stable and chemically inert, have a high dielectric constant, and are suitable for a variety of applications. Dielectric ceramic materials play a vital role in modern technologies, including radar, mobile, military, textiles, sensing systems, spacecraft, etc. In this context, $ZnAl_2O_4$ nanoparticles have been investigated for their possible application in microwave engineering components as filters, resonators, and antennas.

An antenna is a device which radiates electromagnetic waves into space, so it is an essential element employed in transmission devices. Wireless transmission has a higher demand for communication in the present scenario, so the minimization of the antennas is significant.[1] In fabricating microstrip patch antennas (MPAs), $ZnAl_2O_4$ material is suitable owing to its high dielectric permittivity and low tangent loss. By using $ZnAl_2O_4$ nanoparticles, the antenna's size can be reduced while maintaining high performance, making it suitable for use in various wireless communication systems. With these unique properties, $ZnAl_2O_4$ nanoparticles are promising materials for fabricating MPAs with high performance and miniaturization capabilities. Accordingly, various ceramic materials have emerged for microwave applications and are reported in the literature. Ali et al. reported the synthesis of Sn-doped $BaTi_4O_9$ nanoparticles using the mixed oxide route and obtained a smaller grain size

Received: June 6, 2023
Accepted: September 21, 2023
Published: October 5, 2023

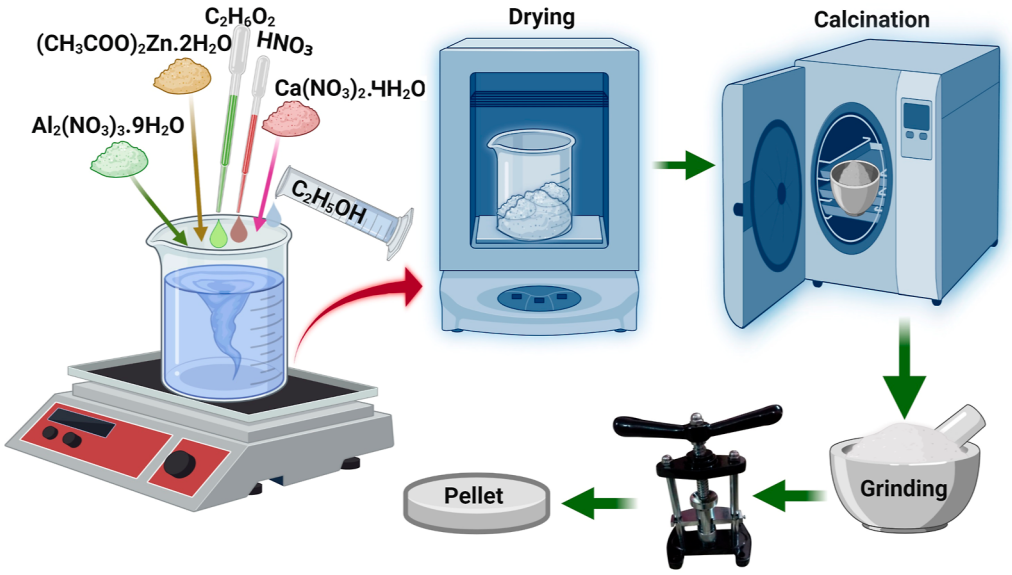

Figure 1. Synthesis process of ceramic nanoparticles with pellet preparation. Reprinted with permission of Springer Nature © 2022.

with an increased Sn concentration. Further, they studied its dielectric characteristics and estimated a dielectric permittivity of 57.29, with a quality factor of 11.852 GHz and tangent loss of 3.007.[2] Similarly, Zak et al. presented the preparation of ZnO nanoparticles using the solvothermal process and explored the analysis. The crystallite and particle sizes were 33 and 48 nm, respectively. They also noticed an absorption peak originated at 370 nm corresponding to an optical band gap of 3.3 eV.[3] Surendran et al. investigated the characteristics of $ZnAl_2O_4$ nanoparticles doped with TiO_2 by the mixed oxide route. The obtained dielectric permittivity was 12.67 with a quality factor of 9950 at a frequency of 10.07 GHz.[4] Mao et al. studied the dielectric properties of $Li_2Mg_3SnO_6$ ceramic nanoparticles after doping with LiF and claimed a dielectric permittivity of 11.13 with a quality factor of 104,750 GHz.[5] Ji et al. prepared $Ca_{(1-x)}SnSiO_{5-x}K_2MoO_4$ composite nanoparticles having a dielectric permittivity of 9.17 with a quality factor of 6240 GHz by the cold sintering process at 180 °C.[6] Yih-Chien Chen et al. employed a solid-state method for preparing $(Mg_{(1-x)}Co_x)_2SnO_4$ ceramic nanoparticles and studied the dielectric properties. The dielectric permittivity, quality factor, and temperature coefficient were 8.8, 110,800 GHz, and −66 ppm/ °C, respectively. The MPA using this material resulted in a return loss of −34.47 and −17.58 dB at resonant frequencies of 2.43 and 5.38 GHz, respectively.[7] Xiong et al. investigated the characteristics of a $0.95MgTiO_3$-$0.05CaTiO_3$ ceramic compound grown by the chemical decomposition reaction approach. The prepared material's dielectric permittivity was 19 with a quality factor of 66,800 GHz. The MPA made up of this material showed a return loss of −24.65 dB at a resonant frequency of 1.5 GHz with a bandwidth of 7 MHz.[8] Similarly, Paulraj and Kalidass employed the composite $MgLa_xFe_{2-x}$ ceramic nanocrystals synthesized by the sol−gel autocomposition method to fabricate the MPA/antenna. They claimed a return loss of −12.85 dB at an operating frequency of 2.4 GHz.[9] So, by adopting a simple synthesis technique, we can alter the dielectric properties of the ceramic to be useful as the substrate material in fabricating a low-profile MPA. Cao et al. studied the dielectric characteristics associated with iron metal oxide content, temperature, and spatial distribution for achieving adjustable microwave absorption performance.[10] Zhang et al. presented the impact of crystal engineering on the electromagnetic attenuation capabilities of bismuth iron cobalt oxide. By employing particular stoichiometry during the synthesis process, the reflection loss was claimed to be −60 dB, indicating its potential application as a superior microwave material for achieving enhanced attenuation performance.[11] Yan et al. presented a straightforward solution-process technique for the growth of perovskite microcrystals and demonstrated the outstanding electromagnetic response across multiple bands.[12] On the other hand, Huang et al. synthesized a composite graphene oxide-based phase change material by adding CuS nanoparticles for enhancing its electromagnetic performance and reported a reduced radar cross-section value of 23.85 dB at a detection angle of 0°.[13] Similarly, Wu et al. explored the comodulation approach of an alkali and Co^{2+} to attain efficient microwave absorption. They obtained an effective absorption bandwidth of 6.72 GHz using an optimized FeCo alloy@porous carbon nanocomposite and also noticed a radar cross-section value of 25.6 dB at an incident angle of 0°.[14] Che et al. prepared carbon and iron-based nanocomposites, and they examined a reflection loss of 25 dB at 11 GHz, which was attributed to the presence of crystalline Fe confined within carbon nanoshells.[15] Liu et al. synthesized $CoNi@SiO_2@TiO_2$ composites and reported exceptional microwave absorption capabilities with a reflection loss of −58.2 dB at a frequency of 10.4 GHz.[16] Similarly, Che et al. prepared carbon nanotube/$CoFe_2O_4$ composites by adopting the chemical vapor deposition method and claimed microwave absorption in the frequency range from 2 to 18 GHz with the potential utility of these composites in the realm of wide-band electromagnetic wave shielding absorbers.[17] In a similar way, Rao et al. synthesized carbon nanotube/$CoFe_2O_4$ nanocomposites that showed the functional properties for absorbing electromagnetic waves in the 2−8 GHz range and claimed a reflection loss of −35.9 dB in the C band.[18]

In this article, we disclose the sol−gel synthesis of Ca-doped $ZnAl_2O_4$ ceramic nanoparticles. The prepared nanoparticles were examined by using various characterization techniques. In a later step, these nanoparticles were cast off as a patch on the FTO substrate to fabricate a prototype MPA. The return loss

https://doi.org/10.1021/acsomega.3c03983
ACS Omega 2023, 8, 38064−38071

of the prototype antenna was measured to be −20.92 dB at a resonance frequency of 6.8 GHz, with a bandwidth of 600 MHz. To our knowledge, there has been no prior study presented on the potential use of this material in fabricating a patch antenna for C-band applications. Section 2 describes the experimental procedure, while the evaluated outcomes are addressed in Section 3. The last part, Section 4, presents a summary of the work.

2. MATERIALS AND METHODS

Ethanol (C_2H_5OH), ethylene glycol ($C_2H_6O_2$), zinc acetate dehydrate ($Zn(O_2CCH_3)_2{\cdot}2H_2O$, purity 99.99%, Lobychem), aluminum nitrate nonahydrate ($Al(NO_3)_3{\cdot}9H_2O$, purity 99.99%, Sigma-Aldrich), calcium nitrate tetra hydrate ($Ca(NO_3)_2H_8O_4$, purity 99.99%, Sigma-Aldrich), and nitric acid (HNO_3) were procured and used as received from the supplier.

The adopted process of the synthesis is illustrated in Figure 1. To synthesize Ca-doped $ZnAl_2O_4$ ceramic nanoparticles, 22.5 g of aluminum nitrate nonahydrate was mixed in absolute ethanol. Further, a chelating agent, ethylene glycol, was added. After 15 min of stirring, 7.704 g of acetate and 4.2 g of calcium nitrate tetrahydrate were added to the above solution. The solution was held for 1 h stirring while the temperature was maintained at the same level. After the addition of 0.36 mL of nitric acid, the solution was turned into a homogeneous state. Further, stirring was continued for 1 h to get a gel, which was dried in an oven, and then thermally treated at 800 °C.

The powder sample was investigated using various characterization techniques, which include X-ray diffraction (XRD, X-Pert Pro, UK), Fourier-Transform Infrared Spectroscopy (BWTEK, Japan), and transmission electron microscopy (TEM, TALOS F200S G2, USA) attached with energy dispersive X-ray spectroscopy (EDS). The powder sample was pressed into a pellet to study the dielectric property using an LCR meter (PSM1735 N4L, Newtons fourth Ltd., UK). The performance of the prototype MPA/antenna was evaluated using a Vector network analyzer (VNA, R&S, ZVL, Germany).

3. RESULTS AND DISCUSSION

Ca-doped $ZnAl_2O_4Ca$ ceramic nanocrystal is a compound formed by incorporating calcium (Ca) into the $ZnAl_2O_4$ ceramic structure while the crystal structure of $ZnAl_2O_4Ca$ remains similar to the parent compound $ZnAl_2O_4$, which is a spinel-type structure. The incorporation of Ca does not significantly alter the overall crystal structure but introduces localized structural changes due to the presence of Ca ions within the crystal lattice. This doping mechanism enhances the material's properties and performance. We conducted an XRD investigation to investigate the crystallinity and crystalline structure of $ZnAl_2O_4Ca$. The XRD pattern of the ceramic nanoparticles scanned between Bragg angles 2θ = 20 and 70° is shown in Figure 2.

The peaks evidenced at Bragg angles 2θ = 31.23, 36.83, 44.80, 47.85, 49, 55.65° and 59.34, 62.23, and 65.25° were described to the planes (220), (311), (400), (331), (422), (511), (440) and (531), respectively.[19] This result coincides with JCPDS File no. 005−0669 of $ZnAl_2O_4$. Using Scherrer's equation, the estimated crystallite size of $ZnAl_2O_4Ca$ was 9.2 nm. In addition, peaks originating at 2θ = 34.36, 47.46, and 62.75° were found to be related to ZnO, having planes of

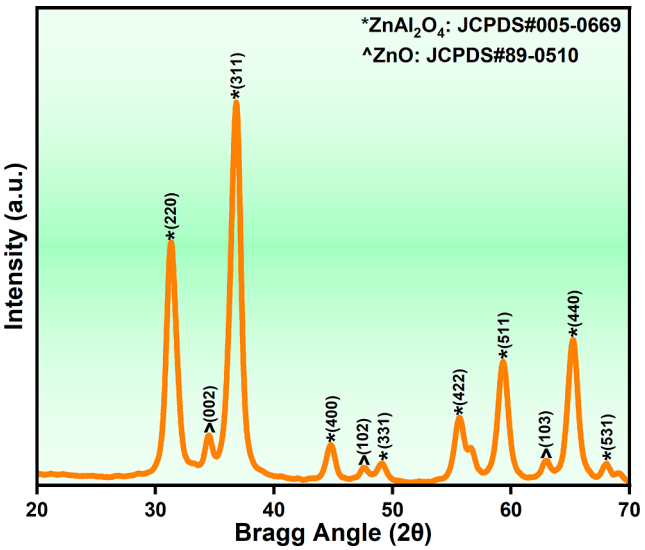

Figure 2. XRD pattern of $ZnAl_2O_4Ca$ ceramic nanocrystals.

(002), (102), and (103), respectively. The XRD analysis reveals that $ZnAl_2O_4Ca$ maintains its crystalline structure even after being doped with Ca, with no observable changes in the crystal arrangement. Moreover, the XRD analysis did not show any CaO impurities resulting from the doping of Ca^{2+}.

The FTIR spectra of the prepared ceramic nanoparticles are shown in Figure 3. A broadband peak observed from 3719 to

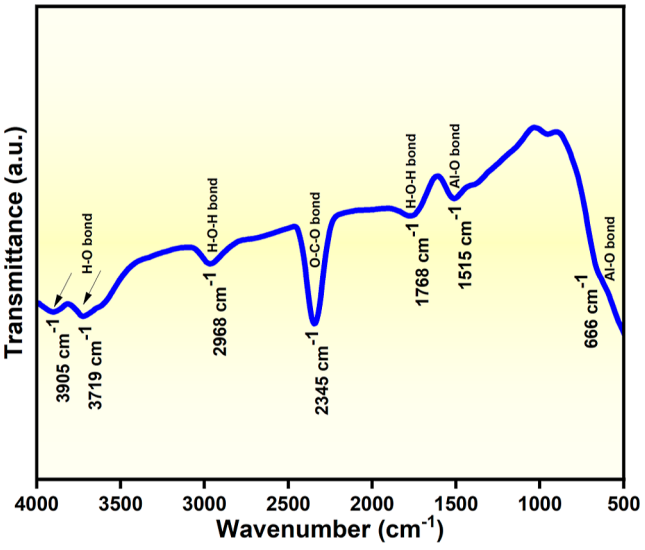

Figure 3. FTIR spectrum of $ZnAl_2O_4Ca$ ceramic nanoparticles.

3905 cm^{-1} represents the vibration band of the oxygen and hydrogen bonds, which is related to the moisture. Other peaks, identified at 1768 and 2345 cm^{-1}, represent the oxygen bonds, while a stretching vibration peak at 1515 cm^{-1} is identified as the Al−O bond.[20] A stretching vibration band of aluminum and oxygen was also noticed at a wavenumber of 666 cm^{-1}. A stretching mode peak, Zn-O-Al of ZnO is anticipated from 420 to 464 cm^{-1}, not shown here. The prepared ceramic nanoparticles contain both oxygen and hydrogen bonds, and the Al−O bond resembles the spinel structure with octahedral coordination occupancy of Al.

https://doi.org/10.1021/acsomega.3c03983
ACS Omega 2023, 8, 38064−38071

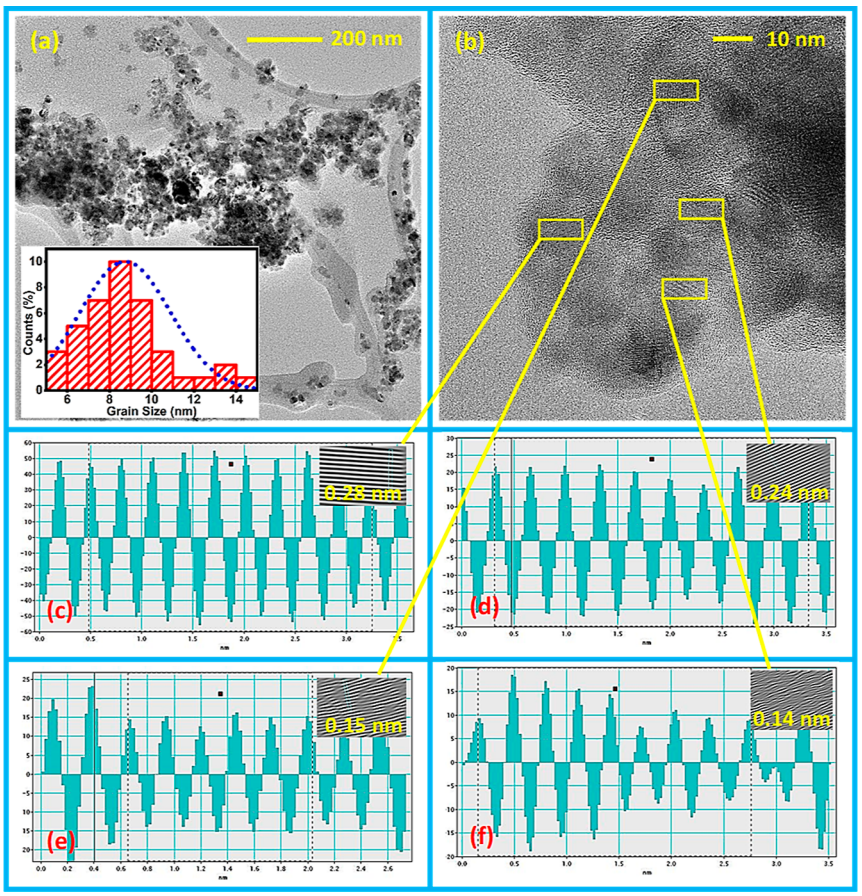

Figure 4. TEM, HRTEM, inverse FFT lattice images with line-profile of $ZnAl_2O_4Ca$ ceramic nanoparticles. TEM micrograph (a) with an inset histogram for estimating the mean particle diameter, HRTEM image (b) with yellow boxes for the analysis, and line-profile with an inset inverse FFT Figure (c–f).

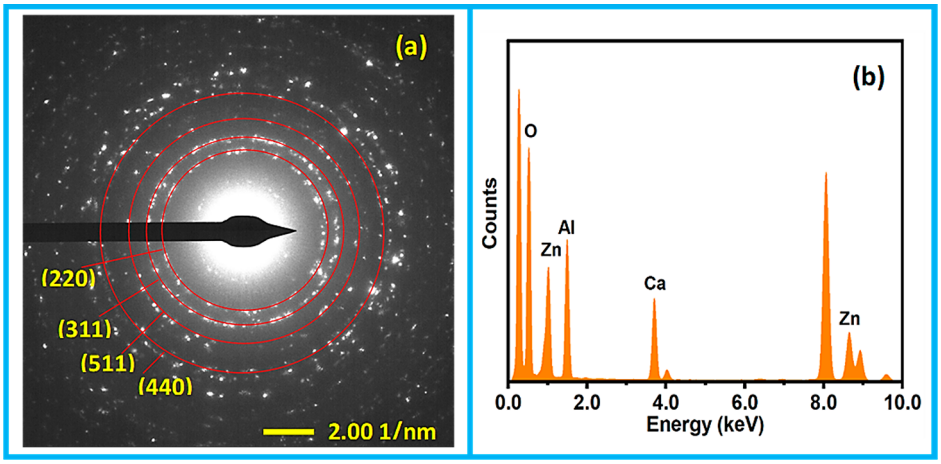

Figure 5. Selected-area electron diffraction and EDS spectrum of $ZnAl_2O_4Ca$ ceramic nanoparticles. SAED pattern (a) and EDS spectrum (b).

Ca-doped $ZnAl_2O_4$ ceramic nanocrystals exhibit a specific microstructure characterized by their composition and arrangement at the nanoscale. Furthermore, the choice of synthesis methods, dopant concentration, and postprocessing treatments play crucial roles in determining their microstructure and properties. Due to their nanocrystalline nature, the Ca-doped $ZnAl_2O_4Ca$ ceramic nanocrystals possess a relatively larger surface area compared to bulk materials. This increased surface area facilitates interactions with other substances and enhances catalytic and functional properties. Material properties are influenced by its microstructure, which includes the arrangement, distribution, and characteristics of its constituents. Physical, mechanical, thermal, electrical, optical, and chemical characteristics are all part of a material's properties. Grain size affects the mechanical strength, hardness, and deformation behavior. Crystal structure determines the mechanical, electrical, and thermal properties. Phase transformation and distribution affect properties such as hardness, strength, conductivity, and reactivity.

https://doi.org/10.1021/acsomega.3c03983
ACS Omega 2023, 8, 38064−38071

Figure 4 depicts the TEM and HRTEM micrographs with inverse FFT lattice images and line-profile of the $ZnAl_2O_4Ca$ ceramic nanoparticles using the freeware Gatan Microscopy Suite. Figure 4a depicts the TEM image of the agglomerated spherical ceramic nanoparticles. The inset histogram depicts the distribution of grains plotted by measuring 40 grains to determine their average size. The TEM investigation evidently showed the grain's mean diameter of 8.13 nm. The high-resolution TEM image showed a clear impression of lattice planes, while some areas are highlighted by the yellow boxes as depicted in Figure 4b. By choosing some areas of the nanoparticles, we conducted the inverse FFT process of the lattices and line-profiling to estimate the *d*-spacing values, as shown in Figure 4c–f. The distance between the planes were found to be 0.28, 0.24, 0.15, and 0.14 nm corresponding to the crystalline planes (220), (311), (511), and (440), respectively. Figure 5a,b) shows the selective-area electron diffraction (SAED) pattern and EDS spectrum. The SAED pattern in Figure 5a reveals the characteristic reflection rings of the polycrystalline nanoparticles. Predominantly, four concentric reflections are prominently identified and successfully matched with the indexing of the crystalline planes (220), (311), (511), and (440). The anticipated compositional elementals, such as Zn, Al, O, and Ca, were observed in the EDS spectrum and are shown in Figure 5b.

The dielectric characteristics of the prepared sample were studied at 30 °C. Figure 6 depicts the dielectric permittivity of

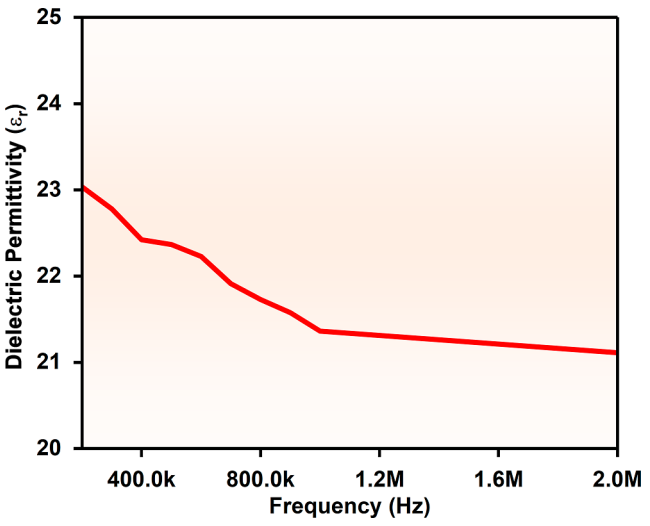

Figure 6. Dielectric permittivity of $ZnAl_2O_4Ca$ ceramic nanoparticles.

the $ZnAl_2O_4Ca$ nanoparticles. The frequency-dependent decrease in dielectric permittivity is a typical characteristic of dielectrics. This decreased dielectric permittivity is related to the dipole polarizations interrupting the dipole arrangement. A high dielectric permittivity at a lower frequency relates to the dipolar orientation, similar to the charge conservation at the junction. At high frequencies, the dipole has no charge accumulation at the interface. Due to this, a low dielectric permittivity was noticed.[2,21] The dielectric permittivity of the $ZnAl_2O_4Ca$ sample was 23.03 at a frequency of 200 kHz and 21.11 at 2 MHz.

Dielectric loss is a factor that is the ratio of dielectric permittivity to the dissipation factor and is called the resistive energy.

The dielectric loss of $ZnAl_2O_4Ca$ ceramic nanoparticles as a function of frequency from 200 kHz to 2 MHz is shown in Figure 7. The polarization of the dipole movement reveals

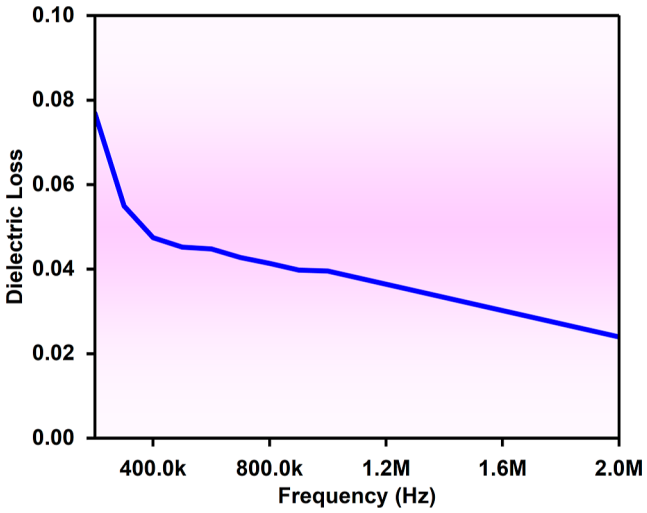

Figure 7. Dielectric loss of the $ZnAl_2O_4Ca$ ceramic nanoparticles.

tangent loss. The long-range movement of electrons decreases at higher frequencies. This may occur because of conduction loss.[22,23] The frequency increases cause a decrease in the dielectric loss. At a frequency of 200 kHz, the tangent loss was 0.077, and it was further reduced to 0.024 at 2 MHz.

Figure 8 shows the ac conductivity of the $ZnAl_2O_4Ca$ ceramic nanoparticles. The ac conductivity of the prepared

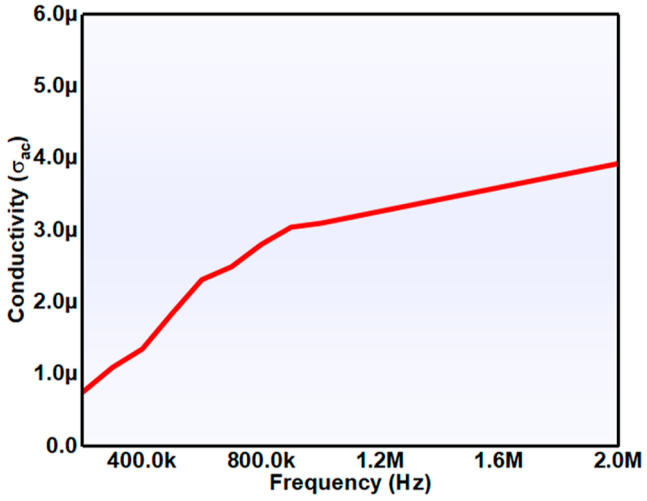

Figure 8. Conductivity of $ZnAl_2O_4Ca$ ceramic nanoparticles.

material is dependent on the frequency. The ac conductivity (σ_{ac}) value increased with the raised frequency.

Due to the space charge and misalignment of cations, the conductivity increases with increasing frequency.[21,24,25] The conductivities were noted to be 1.43 and 4.03 $\mu\Omega^{-1}$ cm^{-1}, corresponding to operating frequencies of 200 kHz and 2 MHz, respectively.

Figure 9 illustrates the construction and fabrication process of a prototype MPA by employing the as-prepared ceramic nanoparticles. A patch of $ZnAl_2O_4Ca$ material was cast on the FTO glass substrate by the doctor blade method. This was

https://doi.org/10.1021/acsomega.3c03983
ACS Omega 2023, 8, 38064−38071

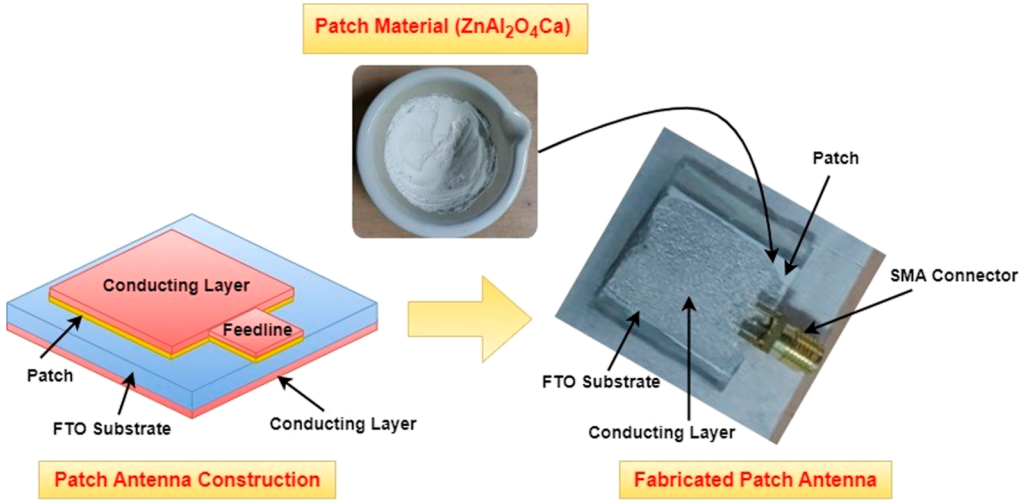

Figure 9. Patch antenna fabrication approach using prepared $ZnAl_2O_4Ca$ ceramic nanoparticles.

followed by contact layer preparation on the $ZnAl_2O_4Ca$ patch and backside of the substrate, and an SMA connector was connected. The prototype MPA's dimensions were 25 mm by 20 mm.

The return loss of the prototype MPA was measured between 4 and 8 GHz as shown in Figure 10. This antenna has

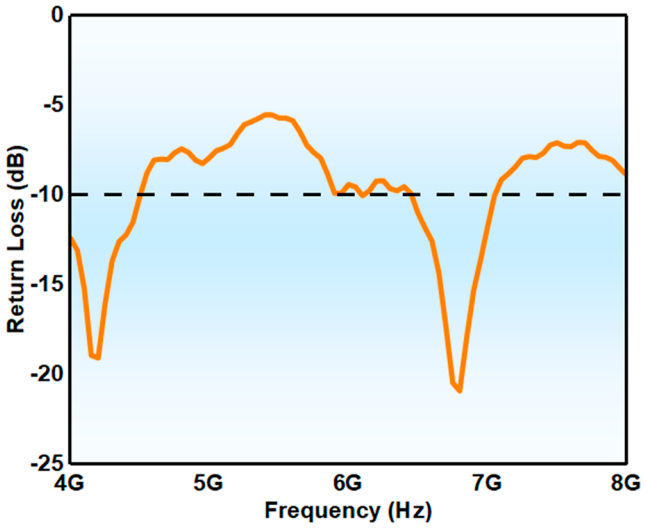

Figure 10. Return loss of $ZnAl_2O_4Ca$ nanoparticle-based prototype patch antenna.

validated optimal return loss below −10 dB. The lowest amount of return loss represents that the antenna allows the maximum energy to be delivered to the load. The prototype microstrip antenna evidenced a return loss of −20.92 dB at a resonance frequency of 6.8 GHz with a bandwidth of 600 MHz. In addition, we also observed another return loss of −19.08 dB at a resonant frequency of 4.2 GHz. Notably, the dominant return loss obtained at a frequency of 6.8 GHz indicates the material's applicability as a substrate for C-band communication.

Voltage standing wave ratio (VSWR) is a significant parameter of the antenna, which refers to the amount of input power reflected from the antenna. This happens when the source impedance equals the impedance of the transmitting antenna.[7] We plotted the VSWR, as shown in Figure 11. For

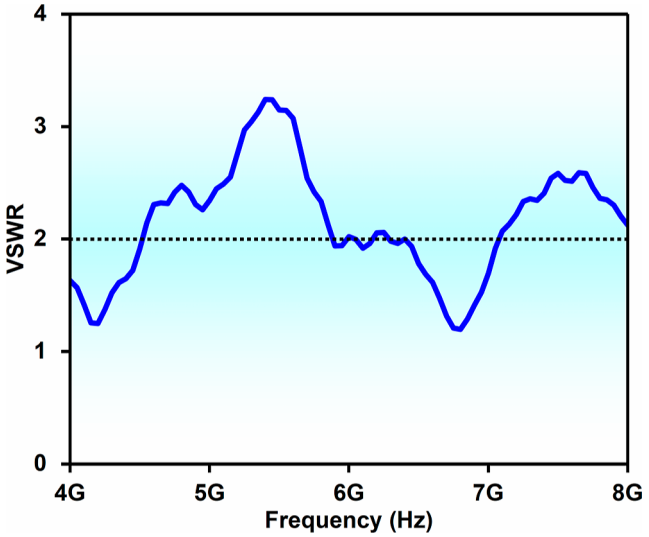

Figure 11. Voltage standing wave ratio of a $ZnAl_2O_4Ca$-based prototype patch antenna.

practical applications, the VSWR of an antenna should be less than 2. At the 6.78 and 4.17 GHz resonance frequencies, the estimated VSWR values were 1.18 and 1.24, respectively. These VSWR values below the minimum required value indicate good characteristics of the prototype MPA for C-band applications.

4. CONCLUSIONS

The synthesis of ceramic nanoparticles of $ZnAl_2O_4Ca$ was successfully carried out, and the nanoparticles were characterized using various techniques such as XRD, FTIR, TEM, and LCR meter. The XRD pattern analysis revealed that the Ca doping did not cause any significant deviation in the Bragg peak position, indicating the successful incorporation of Ca into the $ZnAl_2O_4$ lattice. The FTIR analysis confirmed the presence of functional groups in the prepared nanomaterial. The TEM micrographs revealed that the nanoparticles were spherical in shape, with an average grain diameter of 16 nm. The dielectric permittivity and tangent loss values were decreased from 23.03 to 21.11 and 0.077 to 0.024, respectively, indicating the potential of these nanoparticles for microwave

https://doi.org/10.1021/acsomega.3c03983
ACS Omega 2023, 8, 38064−38071

applications. A prototype antenna fabricated by using these nanoparticles showed a return loss of −20.92 dB at the resonant frequency of 6.8 GHz with a bandwidth of 600 MHz, making it suitable for C-band communication. Additionally, a resonant peak was observed at a frequency of 4.24 GHz, indicating the possibility of fabricating a dual-band antenna. Overall, these results suggest that Ca-doped $ZnAl_2O_4$ ceramic nanoparticles have great potential for use in fabricating MPA applications.

AUTHOR INFORMATION

Corresponding Author

Raghvendra Sarvjeet Dubey − *University Institute of Engineering & Technology, Guru Nanak University, Hyderabad, Telangana State 501506, India; Department of Electronics & Communication Engineering, Guru Nanak Institutions Technical Campus, Hyderabad, Telangana State 501506, India;* orcid.org/0000-0003-1152-7257; Email: deanrnd.uiet@gnuindia.org, rag_pcw@yahoo.co.in

Authors

Sekhar Didde − *Department of ECE, Koneru Lakshmaiah Education Foundation, Guntur, Andhra Pradesh 520002, India; Department of Electronics & Communication Engineering, Swarnandhra College of Engineering and Technology, Narsapur, Andhra Pradesh 534280, India*

Sampad Kumar Panda − *Department of ECE, Koneru Lakshmaiah Education Foundation, Guntur, Andhra Pradesh 520002, India*

Gandla Satheesh Babu − *Interdisciplinary Research Center, RV College of Engineering, Bangalore, Karnataka 560059, India*

Complete contact information is available at: https://pubs.acs.org/10.1021/acsomega.3c03983

Notes

The authors declare no competing financial interest.

REFERENCES

(1) Manas, R. J.; Guru, P. M.; Amiya, B. S.; Mangaraj, B. B. Fractal Geometry and Its Application to Antenna Designs. *International Journal of Engineering and Advanced Technology (IJEAT)*; ISSN, 2019; Vol. *9*, pp 2249−8958.

(2) Ali, A.; Uddin, S.; Lal, M.; Zaman, A.; Iqbal, Z.; Althubeiti, K. Structural, optical and microwave dielectric properties of Ba-$(Ti_{1-x}Sn_x)_4O_9$, $0 \le x \le 0.7$ ceramics. *Sci. Rep.* **2021**, *11*, 17889.

(3) Zak, A. K.; Razali, R.; Abd Majid, W. H. B.; Darroudi, M. Synthesis and characterization of a narrow size distribution of zinc oxide nanoparticles. *Int. J. Nanomed.* **2011**, *6*, 1399−1403.

(4) Surendran, K. P.; Santha, N.; Mohanan, P.; Sebastian, M. T. Temperature stable low loss ceramic dielectrics in (1-x)-$ZnAl_2O_{4-x}TiO_2$ system for microwave substrate applications. *Eur. Phys. J. B* **2004**, *41*, 301−306.

(5) Mao, Y. X.; Pan, H. L.; Zhang, Y. W.; Liu, Q. Q.; Wu, H. T. Effects of LiF addition on the sintering behavior and microwave dielectric properties of $Li_2Mg_3SnO_6$ ceramics. *J. Mater. Sci.: Mater. Electron.* **2017**, *28*, 13278.

(6) Ji, Y.; Song, K.; Zhang, S.; Lu, Z.; Wang, G.; Li, L.; Zhou, D.; Wang, D.; Reaney, I. M. Cold sintered, temperature-stable $CaSnSiO_5$-K_2MoO_4 composite microwave ceramics and its prototype microstrip patch antenna. *J. Eur. Ceram. Soc.* **2021**, *41* (1), 424−429. ISSN 0955−2219

(7) Yih-Chien, C. Microwave dielectric properties of (Mg(1-x)Cox)2SnO4 ceramics for application in dual- band inverted-E-shaped monopole antenna. *IEEE Trans. Ultrason. Ferroelectrics Freq. Control* **2011**, *58* (12), 2531−2538.

(8) Xiong, Z. X.; Zhang, G. F.; Xue, H.; Huang, J. B.; Zheng, Q.; You, B. Q. Dielectric Properties and Microstrip Patch Antenna Performances of $0.95MgTiO_3$-$0.05CaTiO_3$ Microwave Ceramics. *Adv. Mater. Res.* **2013**, *706*−*708*, 64−68.

(9) Paulraj, R. K.; Kalidass, R. Design of Microstrip Patch Antenna Using Lanthanum Doped Magnesium Ferrite Dielectric Materials. *Trans. Electr. Electron. Mater.* **2020**, *21*, 489−496.

(10) Cao, M.-S.; Shu, J.-C.; Wen, B.; Wang, X.-X.; Cao, W.-Q. Genetic Dielectric Genes Inside 2D Carbon-Based Materials with Tunable Electromagnetic Function at Elevated Temperature. *Small Struct.* **2021**, *2*, 2100104.

(11) Zhang, M.; Cao, M. S.; Wang, Q. Q.; Wang, X. X.; Cao, W. Q.; Yang, H. J.; Yuan, J. A multifunctional stealthy material for wireless sensing and active camouflage driven by configurable polarization. *J. Mater. Sci. Technol.* **2023**, *132* (1), 42−49.

(12) Yan, J.; Zheng, Q.; Wang, S.; Tian, Y.; Gong, W.; Gao, F.; Qiu, J.; Li, L.; Yang, S.; Cao, M. Multifunctional Organic-Inorganic Hybrid Perovskite Microcrystalline Engineering and Electromagnetic Response Switching Multi-Band Devices. *Adv. Mater.* **2023**, *35*, 2300015.

(13) Huang, Q.; Zhao, Y.; Wu, Y.; Zhou, M.; Tan, S.; Tang, S.; Ji, G. A dual-band transceiver with excellent heat insulation property for microwave absorption and low infrared emissivity compatibility. *Chem. Eng. J.* **2022**, *446* (4), 137279.

(14) Wu, Y.; Tan, S.; Zhang, T.; Zhou, M.; Fang, G.; Ji, G. Alkali and ion exchange co-modulation strategies to design magnetic-dielectric synergistic nano-absorbers for tailoring microwave absorption. *Nano Res.* **2023**, *16*, 8522−8532.

(15) Che, R. C.; Peng, L.-M.; Duan, X. F.; Chen, Q.; Liang, X. L. Microwave Absorption Enhancement and Complex Permittivity and Permeability of Fe Encapsulated within Carbon Nanotubes. *Adv. Mater.* **2004**, *16* (5), 401−405.

(16) Liu, Q.; Cao, Qi.; Bi, H.; Liang, C.; Yuan, K.; She, W.; Yang, Y.; Che, R. CoNi@SiO_2 @TiO_2 and CoNi@Air@TiO_2 Microspheres with Strong Wideband Microwave Absorption. *Adv. Mater.* **2016**, *28* (3), 486−490.

(17) Che, R. C.; Zhi, C. Y.; Liang, C. Y.; Zhou, X. G. Fabrication and microwave absorption of carbon nanotubes/$CoFe_2O_4$ spinel nanocomposite. *Appl. Phys. Lett.* **2006**, *88* (3), 033105.

(18) Rao, L.; Wang, L.; Yang, C.; Zhang, R.; Zhang, J.; Liang, C.; Che, R. Confined Diffusion Strategy for Customizing Magnetic Coupling Spaces to Enhance Low-frequency Electromagnetic Wave Absorption. *Adv. Funct. Mater.* **2023**, *33*, 2213258.

(19) Strachowski, T.; Grzanka, E.; Mizeracki, J.; Chlanda, A.; Baran, M.; Małek, M.; Niedziałek, M. Microwave-Assisted Hydrothermal Synthesis of Zinc-Aluminum Spinel ZnAl2O4. *Materials* **2022**, *15*, 245.

(20) Ding, M.; Wei, Z.; Li, K.; Wu, X.; Shi, J.; Huang, S. Influence of Cr and Mn co-doping on the microstructure and optical properties of spinel structured $Zn_{0.95-x}Cr_{0.05}Mn_xAl_2O_4$ nanoparticles. *J. Ceram. Soc. Jpn.* **2020**, *128* (11), 927−935.

(21) Pradhan, S. K.; Das, S. N.; Bhuyan, S.; Behera, C.; Padhee, R.; Choudhary, R. N. P. Structural, dielectric and impedance characteristics of lanthanum-modified $BiFeO_3$-$PbTiO_3$ electronic system. *Appl. Phys.* **2016**, *122*, 604.

(22) Das, S. N.; Pradhan, S. K.; Bhuyan, S.; Choudhary, R. N. P. Capacitive, resistive and conducting characteristics of bismuth ferrite and lead magnesium niobate based relaxor electronic system. *J. Mater. Sci.* **2017**, *28*, 18913−18928.

(23) Joshi; Mukundrao, G.; Joseph; Anandraj; Kulkarni; Uday, V.; Sudheesh, K. S. Electrical properties of polyvinylidene fluoride/cellulose acetate blend modified by cenosphere. *Indian J. Pure Appl. Phys.* **2019**, *57*, 737−742.

(24) Halder, S.; Parida, K.; Das, S. N.; Pradhan, S. K.; Bhuyan, S.; Choudhary, R. N. P. Dielectric and impedance properties of $Bi(Zn_{2/3}V_{1/3})O_3$ electric material. *Phys. Lett. A* **2018**, *382*, 716.

(25) Awin, E. W.; Sridar, S.; Kousaalya, A. B.; Vendra, S. S. L..; Koroleva, E..; Filimonov, A..; Vakhrushev, S.; Kumar, R. Low

frequency dielectric behavior and AC conductivity of polymer derived $SiC(O)/HfC_xN_{1-x}$ ceramic nanocomposites. *Mater. Chem. Phys.* **2021**, *260*, 124122.

https://doi.org/10.1021/acsomega.3c03983
ACS Omega 2023, 8, 38064−38071